# The Static Polarizability and Second Hyperpolarizability of Fullerenes and Carbon Nanotubes†

**Lasse Jensen***

*Theoretical Chemistry, Materials Science Centre, Rijksuniversiteit Groningen, Nijenborgh 4, 9747 AG Groningen, The Netherlands*

**Per-Olof Åstrand**

*Department of Chemistry, Norwegian University of Science and Technology, N-7491 Trondheim, Norway*

**Kurt V. Mikkelsen**

*Department of Chemistry, University of Copenhagen, Universitetsparken 5, DK-2100 Copenhagen Ø, Denmark*

*Received: February 27, 2004; In Final Form: May 24, 2004*

Utilizing a point-dipole interaction model, we present an investigation of the static polarizability and second hyperpolarizability of fullerenes and carbon nanotubes by varying their structure. The following effects are investigated: (1) the length dependence of the components of the static polarizability, (2) the static second hyperpolarizabilities of $C_{60}$ and $C_{70}$, (3) the symmetry effects on the static second hyperpolarizability, (4) the length dependence of the components of the static second hyperpolarizability, and (5) the diameter dependence of the static second hyperpolarizability. It is demonstrated that the carbon nanotubes exhibit significantly larger second hyperpolarizabilities compared to a fullerene containing the same number of carbon atoms. Furthermore, the calculations show that the carbon nanotubes have a much larger directionality of the static second hyperpolarizability than the fullerenes.

## I. Introduction

The family of carbon nanotubes is a new set of low dimensional structures which since their discovery about a decade ago have generated much enthusiasm and scientific curiosity due to their unique properties and potential applications.[1−27] Carbon nanotubes can be single- or multi-walled tubes and, depending on the radius and folding, can exhibit metallic or semiconductor behavior. The structure of an individual nanotube is given in terms of ($b_1$, $b_2$) which forms the chiral vector $\mathbf{K} = b_1\mathbf{r}_1 + b_2\mathbf{r}_2$, and the vectors $\mathbf{r}_1$ and $\mathbf{r}_2$ are the lattice vectors of the graphite sheet. Many types of carbon nanotubes can be generated by different combinations of the lattice parameters, but two combinations are of general use: (1) the ($b_1$,$b_1$) type which is the arm-chair structure and (2) the ($b_1$,0) type which is the zigzag structure.

The radius and the chiral angle of the nanotube are given by, respectively,[8,11,12,28]

$$R = \frac{a}{2\pi}(b_1^{\,2} + b_2^{\,2} + b_1 b_2)^{1/2} \tag{1}$$

and

$$\phi = tan^{-1}\left(\frac{\sqrt{3}b_2}{2b_1 - b_2}\right) \tag{2}$$

where $a = \sqrt{3}D$ is the lattice constant of graphite and the nearest-neighbor distance is given by $D = 1.42$ Å. In the case of the semiconductor carbon nanotubes, the band gap may be expressed as[8,11,12,28]

$$E_{\text{gap}} = \frac{|t|D}{R} \tag{3}$$

with $t$ equal to $-3.03$ eV. Having a series of carbon nanotubes where the band gap is tunable within the infrared frequency range indicates an obvious candidate for a tunable detector composed of pixels formed by $10^2$ to $10^3$ individual carbon nanotubes.

Potentially more important applications are expected within the area of nonlinear nano-optoelectronic devices based on the nonlinear optical properties of single-walled carbon nanotubes. Having a uniform electric field applied along the symmetry axis of the carbon nanotube is expected to lead to changes in the refractive index, $\Delta n$, where $n$ is the linear refractive index. This is basically due to the Kerr effect where the change is given by[28]

$$\Delta n = -\frac{2\pi}{n}\chi^{(3)}(-\omega; 0, 0, \omega)E^2 \tag{4}$$

where $\chi^{(3)}(-\omega; 0, 0, \omega)$ is the third-order susceptibility and $E$ is the electric field. Assuming that the electric field is around $10^4$ V/cm and using the results from ref 22 we find $\Delta n > 0.03$ which is substantial and comparable to that produced in heterostructures.[22,28] Changes in the third-order susceptibility of carbon nanotubes as a function of structural parameters may be realized as a method of obtaining nano-optical switches by engineering the nonlinear optical properties by a suitable assembly of carbon nanotubes.[1,2,4−14]

Numerous research groups have envisioned the prospects of future technologies, mainly within information technology,

† Part of the "Gert D. Billing Memorial Issue".

* Corresponding author. E-mail: l.jensen@chem.rug.nl. Present address: Department of Chemistry, Northwestern University, 2145 Sheridan Road, Evanston, IL 60208-3113.

10.1021/jp049109+ CCC: $27.50 
Published on Web 00/00/0000 PAGE EST: 6

based on carbon-based functional materials.[29,30] One of these possibilities is centered around the use of optical devices where the intensity dependence of the refractive index is used for all-optical switching.[29] The performance of these devices depends on the nonlinear optical properties of the materials used for the optical device. A basic motivation for these studies concerns the realization of photonic devices that are able to perform logical operations, switching actions, signal processing, and data storage at speeds beyond the ones seen in electronic devices. For the present and the nearby future it is expected that nonlinear materials will play an important role for the technological advances within photonics.

The crucial nonlinear optical property of the material is the nonlinear response to an electric field given by the macroscopic third-order optical susceptibility, $\chi^{(3)}$. The corresponding microscopic third-order nonlinear optical property is the molecular second hyperpolarizability, $\gamma$, and suitable candidates for optical components have large values of $\gamma$.[29,31,32] The general viewpoint concerning the atomistic design of new nonlinear optical materials is that it is crucial to understand the detailed electronic structure of the materials.[33,34]

The calculations of fourth-order molecular properties are carried out routinely for small to medium-sized molecular systems. High-accuracy electronic structure calculations including a large degree of the electronic correlation of fourth-order molecular properties are presently limited to molecules containing a small number of atoms besides hydrogen atoms. On the other hand, Hartree−Fock and density-functional theory (DFT) calculations of higher order molecular properties for large molecular systems have appeared,[35−37] but ab initio calculations of $\gamma$ on systems containing several thousands of atoms have not been presented.

Molecular mechanics models based on classical electrostatics or additive approaches are from a computational point of view many orders of magnitude faster than the corresponding quantum chemical methods, and they are of general interest when considering nanosized systems. Additive methods based on atomic parameters have been used for the isotropic part of the molecular polarizability.[38,39] Additive approaches have also been utilized when modeling the static and frequency-dependent polarizability tensor of organic molecules[40−42] and the second hyperpolarizability.[43] Point dipole interaction (PDI) models[44−46] represent alternative models for obtaining molecular properties where sets of atomic polarizabilities, $\alpha$, interact with each other according to classical electrostatics. Investigations based on the PDI model have appeared for polarizability,[47−54] optical rotation,[55,56] Raman scattering,[57,58] absorption,[59,60] circular dichroism,[61,62] and hyperpolarizabilities.[63−66] Additional developments of the PDI have considered the effects of the damping of interatomic interactions.[54,67−70]

## II. Theory

The induced dipole moment, $\mu_\alpha^{\mathrm{ind}}$, of a molecular system subjected to an external electric field, $E_\beta^{\mathrm{ext}}$, is written as[71,72]

$$\mu_\alpha^{\mathrm{ind}} = \alpha_{\alpha\beta}^{\mathrm{mol}} E_\beta^{\mathrm{ext}} + \frac{1}{2}\beta_{\alpha\beta\gamma}^{\mathrm{mol}} E_\gamma^{\mathrm{ext}} E_\beta^{\mathrm{ext}} + \frac{1}{6}\gamma_{\alpha\beta\gamma\delta}^{\mathrm{mol}} E_\delta^{\mathrm{ext}} E_\gamma^{\mathrm{ext}} E_\beta^{\mathrm{ext}} + \ldots \quad (5)$$

where we have used the Einstein summation convention for repeated Greek subscripts and the molecular response properties are given by the molecular polarizability, $\alpha_{\alpha\beta}^{\mathrm{mol}}$; the molecular first hyperpolarizability, $\alpha_{\alpha\beta\gamma}^{\mathrm{mol}}$; and the molecular second hyperpolarizability $\alpha_{\alpha\beta\gamma\delta}^{\mathrm{mol}}$ where $\alpha$, $\beta$, $\gamma$, $\delta$ denote Cartesian coordinates.

Representing a molecular system as a set of $N$ atom-like interacting particles, the induced atomic dipole moment, $\mu_{I,\alpha}^{\mathrm{ind}}$ is given as

$$\mu_{\mathrm{I},\alpha}^{\mathrm{ind}} = \alpha_{\mathrm{I},\alpha\beta} E_{\mathrm{I},\beta}^{\mathrm{tot}} + \frac{1}{6}\gamma_{\mathrm{I},\alpha\beta\gamma\delta} E_{\mathrm{I},\delta}^{\mathrm{tot}} E_{\mathrm{I},\gamma}^{\mathrm{tot}} E_{\mathrm{I},\beta}^{\mathrm{tot}} \quad (6)$$

where we utilize the definition of $\alpha_{I,\alpha\beta}$, the polarizability of an atom $I$; and $\gamma_{I,\alpha\beta\gamma\delta}$, the second hyperpolarizability of atom $I$.

The vector sum of the external field and the electric fields from all other atoms gives the total electric field, $E_{I,\beta}^{\mathrm{tot}}$, at atom $I$

$$E_{I,\beta}^{\mathrm{tot}} = E_\beta^{\mathrm{ext}} + \sum_{J\neq I}^{N} T_{IJ,\beta\gamma}^{(2)} \mu_{J,\gamma}^{\mathrm{ind}} \quad (7)$$

where the interaction tensor is given as

$$T_{IJ,\beta\gamma}^{(2)} = \frac{3R_{IJ,\beta}R_{IJ,\gamma}}{R_{IJ}^5} - \frac{\delta_{\beta\gamma}}{R_{IJ}^3} \quad (8)$$

where $R_{IJ}$ is the distance between atoms $I$ and $J$ and $R_{IJ,\beta}$ denotes a Cartesian coordinate component of the distance vector.

A different viewpoint is to let the electric field at each atom be an independent variable, and thereby we may expand the atomic induced dipole moment in a Taylor expansion in terms of relay tensors.[73] Thereby, the molecular induced dipole moment is the sum of the atomic induced dipole moments and by assuming that the external field is homogeneous, i.e. $E_{J,\beta}^{\mathrm{ext}} = E_\beta^{\mathrm{ext}}$ for all $J$, we are able to write the molecular induced dipole moment as

$$\mu_\alpha^{\mathrm{ind}} = \Big(\sum_{I,J}^{N} B_{IJ,\alpha\beta}^{(2)}\Big) E_\beta^{\mathrm{ext}} + \frac{1}{2}\Big(\sum_{I,J,K}^{N} B_{IJK,\alpha\beta\gamma}^{(3)}\Big) E_\gamma^{\mathrm{ext}} E_\beta^{\mathrm{ext}} + \frac{1}{6}\Big(\sum_{I,J,K,L}^{N} B_{IJKL,\alpha\beta\gamma\delta}^{(4)}\Big) E_\delta^{\mathrm{ext}} E_\gamma^{\mathrm{ext}} E_\beta^{\mathrm{ext}} + \ldots \quad (9)$$

We are able to identify the molecular (hyper)polarizabilities by comparing the expressions in eqs 5 and 9. We obtain the two-atom relay tensor, $B_{IJ,\alpha\beta}^{(2)}$, as

$$B_{IJ,\alpha\beta}^{(2)} = \alpha_{I,\alpha\gamma}\Big(\delta_{IJ}\delta_{\gamma\beta} + \sum_{K\neq I}^{N} T_{IK,\gamma\delta}^{(2)} B_{KJ,\delta\beta}^{(2)}\Big) \quad (10)$$

which in matrix notation is obtained as[45,68]

$$B^{(2)} = (\boldsymbol{\alpha}^{-1} - \mathbf{T}^{(2)})^{-1} \quad (11)$$

Using the scheme by Sundberg,[73] we obtain the three- and four-atom relay tensors. As demonstrated in ref 66, the four-atom relay tensor for a system of spherically symmetric particles may be written as

$$B_{IJKL,\alpha\beta\gamma\delta}^{(4)} = \sum_{M}^{N} \gamma_{M,\lambda\mu\nu\xi} \tilde{B}_{ML,\xi\delta}^{(2)} B_{MK,\nu\gamma}^{(2)} B_{MJ,\mu\beta}^{(2)} B_{MI,\lambda\alpha}^{(2)} \quad (12)$$

where $\tilde{B}_{IJ,\alpha\beta}^{(2)}$ is defined as

$$\tilde{B}_{IJ,\alpha\beta}^{(2)} = \delta_{IJ}\delta_{\alpha\beta} + \sum_{K\neq I}^{N} T_{IK,\alpha\gamma}^{(2)} B_{KJ,\gamma\beta}^{(2)} \quad (13)$$

Finally, the molecular polarizability, $\alpha_{\alpha\beta}^{\mathrm{mol}}$, and molecular second hyperpolarizability, $\gamma_{\alpha\beta\gamma\delta}^{\mathrm{mol}}$, are given as

$$\alpha_{\alpha\beta}^{\mathrm{mol}} = \sum_{IJ}^{N} B_{IJ,\alpha\beta}^{(2)} \tag{14}$$

and

$$\gamma_{\alpha\beta\gamma\delta}^{\mathrm{mol}} = \sum_{IJKL}^{N} B_{IJKL,\alpha\beta\gamma\delta}^{(4)} \tag{15}$$

For further details on the theoretical background, we refer to our previous work.[66]

An improved model is obtained if the contributions from a smeared-out charge distribution is included in terms of a damping of the interaction in eq 5 by modifying the $T_{IJ,\alpha\beta}$ tensor.[67,68] The damping of the interactions arises from the overlap of the smeared-out charge distributions, and the model used here is obtained by considering the overlap between two Gaussian charge distributions.[54] We obtain the damped interaction by modifying the interaction tensors as

$$T_{IJ,\alpha_1\ldots\alpha_n}^{(n)} = \nabla_{\alpha_1}\ldots\nabla_{\alpha n}\left(\frac{1}{S_{IJ}}\right) \tag{16}$$

which is equivalent to replacing the regular distance $R_{IJ}$ by a scaled distance $S_{IJ}$ and analogously $R_{IJ,\alpha}$ by $S_{IJ,\alpha}$ in the regular formulas for the interaction tensor. We utilize the following scaled distance[54]

$$S_{IJ} = \sqrt{R_{IJ}^2 + \frac{\pi}{4a_{IJ}}} \tag{17}$$

where $a_{IJ}$ is given by $a_{IJ} = \Phi_I\Phi_J/(\Phi_I + \Phi_J)$, and $\Phi_I$ is the damping parameter for atom $I$ corresponding to the exponent in a Gaussian function describing the charge distribution on atom $I$.

**Structures and Parameters.** We have obtained the structures of the small fullerenes and nanotubes at the PM3 level from refs 52 and 74 where the carbon nanotubes have a uniform bond length of 1.42 Å. The atom-type parameters for the calculation of hyperpolarizabilities using the interaction model are taken from our previous work.[54,66,75] Our previous work is based on a large number of quantum chemical calculations at the SCF level of the electronic contribution to the hyperpolarizability tensors; however, the $\gamma$ parameter for carbon used in our studies of carbon fullerenes and nanotubes has been chosen so that the model reproduces the correct second hyperpolarizability for the $C_{60}$ fullerene molecule.[75] The parameters used in this work are $\alpha_C = 9.312$ au, $\Phi_C = 0.124$ au, and $\gamma_C = 1600.0$ au, and in our previous work we have demonstrated that these parameters give reliable results for polarizabilities and hyperpolarizabilities of fullerenes and nanotubes.[54,66,75] The performance of the PDI model has been considerably better than the computed hyperpolarizabilities from various semiempirical methods and the discrepancies compared to the computed molecular hyperpolarizability using quantum chemical calculations are generally around 10% and in all cases below 30%.[66] Improvements of the PDI model are connected to the availability of performing very accurate quantum chemical calculations routinely on medium-sized molecules and therefore provide more accurate parameters for the PDI model. We have previously demonstrated that an atomistic model can be used for calculating molecular hyperpolarizability of carbon nanotubes up to a length where $\gamma$ scales linearly with the length of the tube.[75] Thereby, we have demonstrated that it is possible to use atomistic models to calculate electronic response properties at all relevant length scales.

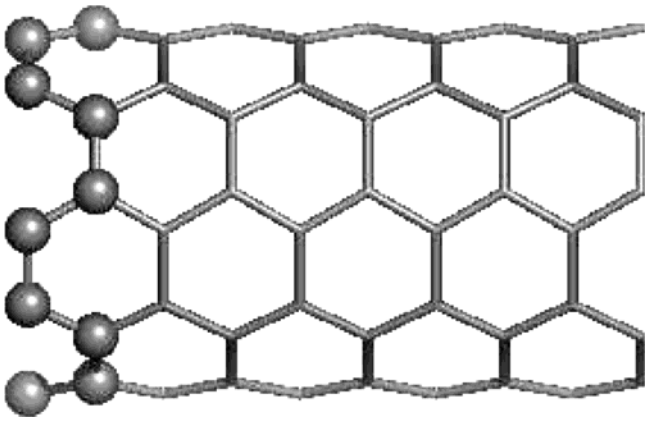

**Figure 1.** A [5,5] nanotube with 100 carbon atoms. The atoms in the unit cell are displayed as spheres.

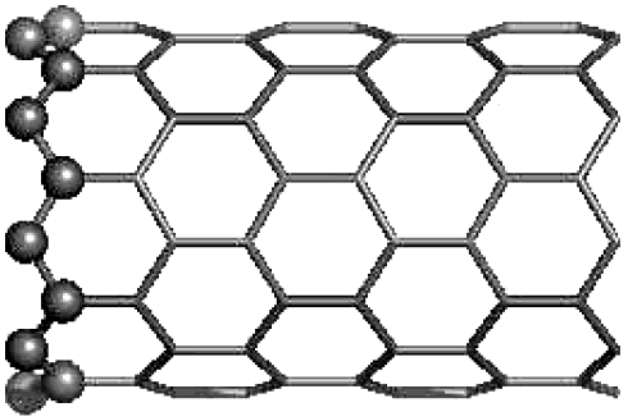

**Figure 2.** A [9,9] nanotube with 108 carbon atoms. The atoms in the unit cell are displayed as spheres.

## III. Results

In Figures 1 and 2, we present the structures of the open-ended [5,5] and [9,0] carbon nanotubes. Results are presented for the average polarizability, $\bar{\alpha}$, given as

$$\bar{\alpha} = \frac{1}{3}(\alpha_{xx} + \alpha_{yy} + \alpha_{zz}) \tag{18}$$

the average hyperpolarizability, $\bar{\gamma}$, given as[76]

$$\bar{\gamma} = \frac{1}{15}\sum_{\alpha,\beta}\gamma_{\alpha\alpha\beta\beta} + \gamma_{\alpha\beta\alpha\beta} + \gamma_{\alpha\beta\beta\alpha} \tag{19}$$

and for the individual components $\alpha_{xx}$, $\alpha_{zz}$, $\gamma_{zzzz}$, $\gamma_{xxxx}$, and $\gamma_{xxzz}$, where the $z$ axis is directed along the tube and the $x$ axis is perpendicular to the tube.

**A. Saturation of the Static Polarizability for Large Nanotubes.** Figure 3 exhibits the length dependence of the static polarizability per unit cell for the [5,5] and the [9,0] carbon nanotubes. The results for $\alpha^{\mathrm{mol}}$ for the [5,5] and [9,0] nanotubes have been characterized by fitting the results to the expression

$$\frac{\alpha(N)}{N} = \alpha^{\infty} - C\exp\left(-\frac{N}{N^{\mathrm{sat}}}\right) \tag{20}$$

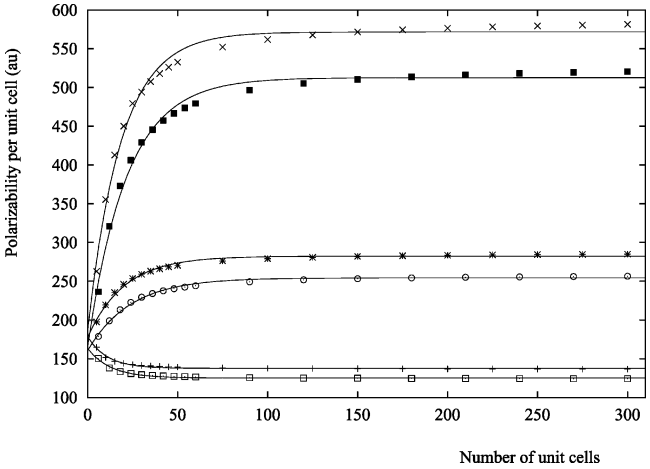


**Figure 3.** Static polarizability per unit cell for [5,5] and [9,0] nanotubes as a function of the number of unit cells (in 1000 au) by increasing the length of the tube. The symbols (×) and (∗) denote *zz* component and mean value, respectively, for the [5,5] nanotube. For the [9,0] nanotube (■) denote the *zz* component and (○) the mean value. The symbols (+) and (□) denote *xx* component for the [5,5] and [9,0] nanotube, respectively. Solid lines are the plot of the corresponding fit.

**TABLE 1: Fitting Parameters for Characterizing Mean Value and Individual Components of the Polarizability for [5,5] and [9,0] Carbon Nanotubes[a]**

| | mean | *zz* | *xx* |
|---|---|---|---|
| | | [5,5] | |
| $N^{sat}$ | 20.22 ± 0.92 | 18.53 ± 0.99 | 10.95 ± 0.90 |
| $\alpha^{\infty}$ | 282.29 ± 0.75 | 571.57 ± 3.06 | 137.63 ± 0.33 |
| C | 104.54 ± 3.1 | 384.99 ± 13.83 | 40.48 ± 2.65 |
| | | [9,0] | |
| $N^{sat}$ | 23.63 ± 1.10 | 21.74 ± 1.17 | 12.78 ± 1.08 |
| $\alpha^{\infty}$ | 254.28 ± 0.70 | 512.59 ± 2.86 | 125.16 ± 0.32 |
| C | 93.57 ± 2.83 | 346.66 ± 12.5 | 37.95 ± 2.56 |

[a] All parameters are in au.

used by Schulz et al. to characterize the saturation of $\alpha^{mol}$ and $\gamma^{mol}$ of organic oligomers.[77] The parameter $\alpha^{\infty}$ represents the asymptotic value and $N^{sat}$ represents the onset where the saturation starts. The parameters for all the fits are displayed in Table 1 and are plotted with solid lines in Figure 3.

The static polarizabilities of the two families of carbon nanotubes reach their saturation levels at lengths of less than 100 unit cells. This observation holds for both the parallel $\alpha_{zz}$ and the perpendicular $\alpha_{xx}$ components with the latter components reaching their saturation levels earlier. The largest increases of the polarizabilities with respect to the length of the carbon nanotube are given by the parallel components. In comparison to our previous work on saturation length for the static second hyperpolarizability of [5,5] and [9,0] carbon nanotubes,[75] the static polarizabilities reach their respective saturation levels at much shorter lengths of the nanotubes. From Figure 3, it is seen that $\alpha_{xx}$ per unit cell decreases slightly with respect to the length of the tube, whereas $\alpha_{zz}$ increases. For the longer tubes, the polarizability per unit cell resembles the cells in the middle of the tube. For the smaller tubes, it resembles both the cells in the middle and in the end of the tube. In the middle of tube the electrons are delocalized much more along the tube than perpendicular to the tube compared with electrons in the end of the tube. Therefore, it is expected that the polarizability should increase along the tube and decrease perpendicular to the tube. Similar trends have been observed for molecular complexes.[54]

The scaling parameters obtained for the nanotubes can be compared with the characterization of a series of conjugated organic oligomers carried out by Schulz et al.[77] The saturation lengths obtained for the oligomers are between ∼1.4−4 nm, in comparison to ∼4.5 nm obtained for the carbon nanotubes in this work. If $\alpha_{zz}^{\infty}$ is considered, a value of ∼238 au/Å is found for both types of nanotubes compared with the values for the conjugated oligomers which vary between ∼33 au/Å and ∼85 au/Å. It is noted that the asymptotic limit of the polarizability for the carbon nanotubes is significantly larger than that of the oligomers. In our previous work on the saturation of the static second hyperpolarizability of carbon nanotubes we found a saturation length of ∼7.5 nm, almost twice the saturation length for the polarizability.[75] This behavior has also been observed for e.g. polyacetylene.[77]

**TABLE 2: Mean Static Second Hyperpolarizability for $C_{60}$ and $C_{70}$ (in au)**

| method | $C_{60}$ | $C_{70}$ | $C_{70}/C_{60}$ | ref |
|---|---|---|---|---|
| PDI | 115198 | 145496 | 1.26 | this work |
| SCF−RPA | 109198 | 149701 | 1.37 | [79]basis set: 6-31++G |
| MNDO/PM3-FF | 49834 | 89741 | 1.80 | 80 |
| AM1/valence-FF | 49040 | 108206 | 2.20 | 81 |
| NDDO/PM3-FF | 64328 | 120913 | 1.88 | 82 |

**B. $\bar{\gamma}$ for $C_{60}$ and $C_{70}$.** $\bar{\gamma}$ of the $C_{60}$ and $C_{70}$ structures are presented in Table 2 which contains results from the present work, ab initio calculations, and semiempirical calculations. Generally, we observe that the PDI and the ab initio results are in good agreement, whereas $\bar{\gamma}$ calculated by different semiempirical methods differ significantly. We have not compared with experiment results since results only exist for the condensed phase, and it is nontrivial to compare calculations on the isolated system with experimental condensed phase values.[78]

In the case of $C_{60}$, the semiempirical results underestimate the magnitude of $\bar{\gamma}$ by a factor 2.19, 2.22, and 1.70 for the MNDO/PM3-FF, AM1/valence-FF, and NDDO/PM3-FF semiempirical methods, respectively, as compared to SCF−RPA calculations. The PDI result for $C_{60}$ is a factor of 1.05 larger than the SCF−RPA results which reflects a relatively good performance of the PDI calculations.

For $C_{70}$, the semiempirical results for $\bar{\gamma}$ are in closer agreement with the ab initio calculations and the PDI results. The ratio between the semiempirical results and the SCF−RPA results are, in the same order of semiempirical methods as above, 1.67, 1.38, and 1.24, respectively. The PDI calculation provides a $\bar{\gamma}$ that is a factor of 0.97 smaller than the SCF−RPA results.

Based on the performance of the semiempirical calculations in relation to the results from the SCF−RPA calculations of $\gamma$, we do not consider the semiempirical results to be sufficiently reliable neither for absolute values nor for scalability of the physical size of the investigated systems. On the other hand, the PDI results for $\bar{\gamma}$ indicate a reliable and inexpensive method for calculating hyperpolarizabilities both with respect to absolute values and size-dependent changes of the magnitudes of $\bar{\gamma}$.

**C. Symmetry Effects on $\gamma$.** From the investigation of the symmetry of the tube, it is observed from the calculations presented in Table 3 that $\gamma$ depends strongly on the number of open ends of the carbon nanotubes. The closing of one end of a tube leads to a substantial decrease in both $\gamma_{xxxx}$ and $\gamma_{zzzz}$. The decrease of $\gamma_{zzzz}$ from open to half-closed or fully closed is 4% and 34%, respectively. For $\gamma_{xxxx}$, the decrease amounts to 6% and 41% for half-closed and fully closed nanotubes, respectively. The average hyperpolarizability, $\bar{\gamma}$, diminishes by 5% and 38% from open to either half-closed or fully closed nanotubes, respectively.

Comparing the two different nanotubes [5,5] and [9,0] reveals for open nanotubes that the perpendicular component are almost equal, whereas the parallel component for [5,5] nanotube is

**TABLE 3: Symmetry Effects on the Static Second Hyperpolarizability for Small Nanotubes (in $10^3$ au)[a]**

| | $\gamma_{xxxx}$ | $\gamma_{zzzz}$ | $\bar{\gamma}$ | $\bar{\gamma}/N$ |
|---|---|---|---|---|
| $[5,5]^0_{90}$ | 245.34 | 653.79 | 366.25 | 4.07 |
| $[5,5]^1_{90}$ | 229.96 | 629.06 | 347.36 | 3.86 |
| $[5,5]^2_{90}$ | 145.50 | 430.84 | 226.30 | 2.51 |
| $[9,0]^0_{90}$ | 245.65 | 603.25 | 350.48 | 3.89 |

[a] Subscript indicates number of carbon atoms in the nanotube and superscript indicates number of closed ends. The *z* axis is along the tube and the *x* axis is perpendicular to the tube.

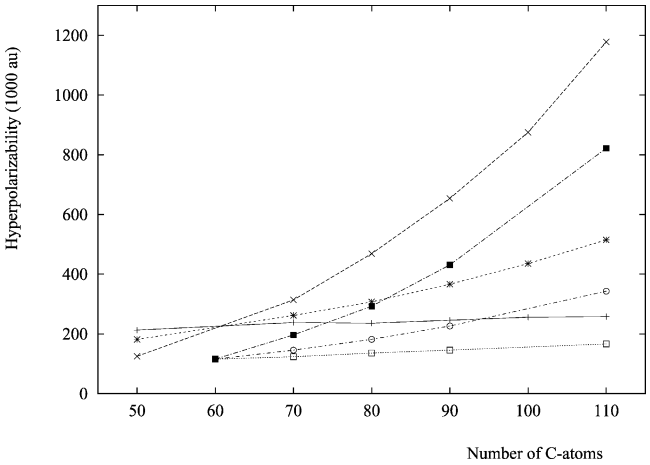


**Figure 4.** Static hyperpolarizability for small fullerenes and [5,5] nanotubes as a function of the number of carbon atoms (in 1000 au) by increasing the length of the tube. (×) $\gamma_{zzzz}$ for [5,5] nanotubes, (+) $\gamma_{xxxx}$ for [5,5] nanotubes, (∗) $\bar{\gamma}$ for [5,5] nanotubes, (■) $\gamma_{zzzz}$ for fullerenes, (□) $\gamma_{xxxx}$ for fullerenes, and (○) $\bar{\gamma}$ for fullerenes.

about 8% larger than for the [9,0] carbon nanotube. The difference in $\bar{\gamma}$ between the two types of nanotubes is less than 5%, and also for $\bar{\gamma}/N$ the difference is less than 5%.

**D. The Static Hyperpolarizability for Nanotubes and Fullerenes.** In Figure 4, we present the static hyperpolarizabilities for small fullerenes and [5,5] carbon nanotubes as a function of the number of carbon atoms. Generally, the $\gamma_{zzzz}$ component for the [5,5] nanotubes is about 50% larger than the $\gamma_{zzzz}$ component for the fullerenes containing the same number of carbon atoms. The $\gamma_{xxxx}$ component for the [5,5] nanotubes increases by ∼20%, whereas for the fullerenes the increase is larger and around 50%. For a given number of carbon atoms, $\bar{\gamma}$ is significantly larger for the nanotubes than for the fullerenes, and the difference increases with the number of carbon atoms. Carbon nanotubes provide for a given number of carbon atoms a much larger hyperpolarizability along the length of the nanotube. Carbon nanotubes have a directionally governed hyperpolarizability.

**E. Diameter Effects $\gamma$.** The dependence of the static hyperpolarizability on the diameter of the tube is presented in Figures 5 and 6 for a series of armchair ([5,5] − [10,10]) and zigzag ([9.0] − [18,0]) carbon nanotubes with the same length. The length of the armchain tubes are 9.8 Å and for the zigzag tubes 8.5 Å. For both series of carbon nanotubes, the $\gamma_{xxxx}$ component increases strongly as the diameter is increased through the addition of carbon atoms, a larger diameter relates to a larger number of carbon atoms perpendicular to the length of the carbon nanotube. For the armchair carbon nanotubes, the perpendicular component $\gamma_{xxxx}$ becomes larger than the parallel component for the [10,10] nanotube. In the case of the zigzag carbon nanotubes, the $\gamma_{xxxx}$ becomes larger than the $\gamma_{zzzz}$ component for the [14,0] nanotube. According to eq 1, the

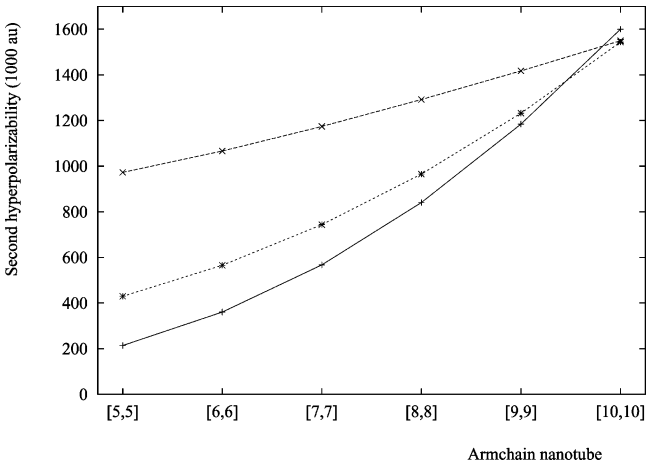


**Figure 5.** Static hyperpolarizability for small armchair nanotubes as a function of the number of carbon atoms (in 1000 au) by increasing the diameter of the tube. (×) $\gamma_{zzzz}$, (+) $\gamma_{xxxx}$, and (∗) $\bar{\gamma}$.

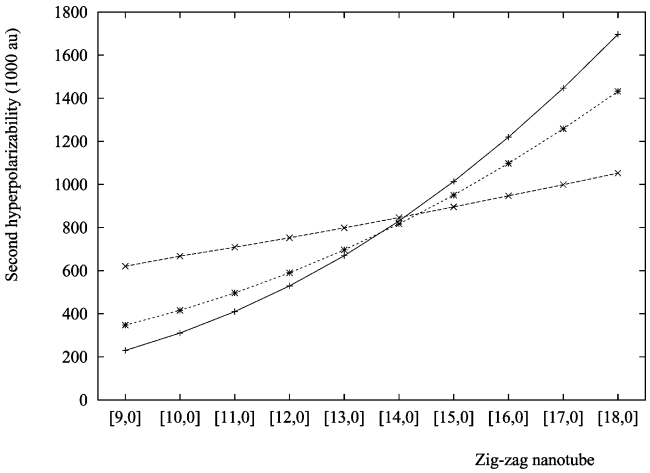


**Figure 6.** Static hyperpolarizability for small zigzag nanotubes as a function of the number of carbon atoms (in 1000 au) by increasing the diameter of the tube. (×) $\gamma_{zzzz}$, (+) $\gamma_{xxxx}$, and (∗) $\bar{\gamma}$.

[10,10] has a diameter of ∼13.5 Å and the [14,0] a diameter of ∼11 Å. Therefore, for both tubes the diameter of the tube has to be larger than the length of the tube before the perpendicular component becomes more important.

Extending the diameter for a given family of carbon nanotubes provides not only a substantial increase in $\gamma_{xxxx}$ but also a large increase in $\gamma_{zzzz}$ which leads to that $\bar{\gamma}$ increases remarkably with the number of carbon atoms.

## IV. Conclusion

We have shown that the PDI model provides static hyperpolarizabilities for $C_{60}$ and $C_{70}$ that are comparable to ab initio wave function methods. Additionally, the scaling of the hyperpolarizability going from $C_{60}$ to $C_{70}$ is reproduced well by the PDI model.

Furthermore, the PDI model demonstrates the significant decrease of the static hyperpolarizability as the carbon nanotubes are closed in one or two ends. The static hyperpolarizabilities are significantly larger along the tube for the [5,5] nanotubes than for the [9,0] nanotubes, whereas the perpendicular components are of similar magnitude.

Compared to our previous work on saturation lengths for hyperpolarizabilities of carbon nanotubes,[75] we have demonstrated here that the static polarizability reach their saturation levels at much shorter lengths of the tubes.

We have performed a comparison between the hyperpolarizabilities of the small fullerenes and the [5,5] nanotubes. For a given number of carbon atoms the hyperpolarizabilities of the carbon nanotubes are larger than the ones for the fullerenes. It is also clear that the nanotubes have a much larger directionality of the second hyperpolarizability tensor.

Finally, we have shown the effects on the hyperpolarizabilities of increasing the diameter of armchair and zigzag nanotubes. The hyperpolarizabilities increase with larger diameter where $\gamma_{xxxx}$ obviously increases the most but $\gamma_{zzzz}$ also increases. In the case of the zigzag nanotubes the crossover (the diameter where $\gamma_{xxxx} > \gamma_{zzzz}$) occurs for smaller diameters than for the armchair nanotubes.

**Acknowledgment.** L.J. gratefully acknowledges The Danish Research Training Council for financial support. P.-O.Å. has received support from the Norwegian Research Council (NFR) through a Strategic University Program (Grant no. 154011/420), a NANOMAT program (Grant no. 158538/431), and a grant of computer time from the Norwegian High Performance Computing Consortium (NOTUR). K.V.M. thanks Statens Naturvidenskabelige Forskningsråd (SNF), Statens Teknisk-Videnskabelige Forskningsråd (STVF), Dansk Center for Scientific Computing, and the EU-networks: MOLPROP and THEONET II for support.

## References and Notes

(1) Ebbesen, T. W. *Annu. Rev. Mater. Sci.* **1994**, *24*, 235.
(2) Dresselhaus, M.; Dresselhaus, G.; Eklund, P. C. *Science of Fullerenes and Carbon nanotubes*; Academic Press,: San Diego, 1996.
(3) Saito, R.; Dresselhaus, G.; Dresselhaus, M. *Physical Properties of Carbon nanotubes*; Imperical College Press: London, 1998.
(4) Iijima, S.; Ichihashi, T. *Nature* **1993**, *363*, 603.
(5) Seraphin, S.; D. Zhou, D. *Appl. Phys. Lett.* **1994**, *64*, 2087.
(6) Treacy, M. M. J.; Ebbesen, T. W.; Gibson, J. M. *Nature* **1996**, *381*, 678.
(7) Kane, C. L.: Mele, E. J. *Phys. Rev. Lett.* **1997**, *78*, 1932.
(8) Jiang, J.; Dong, J.; Xing, D. Y. *Phys. Rev. B* **1999**, *59*, 9838.
(9) Sun, Y.-P.; Fu, K. F.; Lin, Y.; Huang, W. J. *Acc. Chem. Res.* **2002**, *35*, 1096.
(10) Zhou, O.; Shimoda, H.; Gao, B.; Oh, S. J.; Fleming, L.; Yue, G. Z. *Acc. Chem. Res.* **2002**, *35*, 1045.
(11) Ouyang, M.; Huang, J. L.; Lieber, C. M. *Acc. Chem. Res.* **2002**, *35*, 1018.
(12) Slepyan, G. Ya.; Maksimenko, S. A.; Kalosha, V. P.; Herrmann, J.; Campbell, E. E. B.; Hertel, I. V. *Phys. Rev. A* **1999**, *60*, R777.
(13) J. M. Pitarke, J. M.; Carcia-Vidal, F. J. *Phys. Rev. B* **2001**, *63*, 073404.
(14) Qu, S. L.; Du, C. M.; Song, Y. L.; Wang, Y. X.; Gao, Y. C.; Liu, S. T.; Li, Y. L.; Zhu, D. B. *Chem. Phys. Lett.* **2002**, *356*, 403.
(15) Slepyan, G. Ya.; Maksimenko, S. A.; Kalosha, V. P.; Gusakov, A. V.; Herrmann, J. *Phys. Rev. A* **2001**, *63*, 053808.
(16) Machon, M.; Reich, S.; Thomsen, C.; Sanchez-Portal, D.; Ordejon, P. *Phys. Rev. B* **2002**, *66*, 155410.
(17) Han, H.; Vijayalakshmi, S.; Lan, A.; Iqbal, Z.; Grebel, H.; Lalanne, E.; Johnson, A. M. *Appl. Phys. Lett.* **2003**, *82*, 1458.
(18) Avouris, P. *Acc. Chem. Res.* **2002**, *35*, 1026−1034.
(19) Liang, W. Z.; Wang, X. J.; Yokojima, S.; Chen, G. H. *J. Am. Chem. Soc.* **2000**, *122*, 11129.
(20) Cioslowski, J.; Rao, N.; Moncrieff, D. *J. Am. Chem. Soc.* **2002**, *124*, 8485.
(21) Slepyan, G. Ya.; Maksimenko, S. A.; Lakhtakia, A.; Yevtushenko, O. M. *Synth. Met.* **2001**, *124*, 121.
(22) Margulis, Vl. A.; Gaiduk, E. A.; Zhidkin, E. N. *Opt. Commun.* **2000**, *183*, 317.
(23) Margulis, Vl. A.; Sizikova, T. A. *Physica B* **1998**, *245*, 173.
(24) Vivien, L.; Riehl, D.; Hache, F.; Anglaret. E. *Physica B* **2002**, *323*, 233.
(25) Vivien, L.; Lancon, P.; Riehl, D.; Hache, F.; Anglaret. E. *Carbon* **2002**, *40*, 1789.
(26) Cohen, M. L. *Solid State Comm.* **1998**, *107*, 589.
(27) Poulin, P.; Vigolo, B.; Launois, P. *Carbon* **2002**, *40*, 1741.
(28) Dragoman, D.; Dragoman, M. *Prog. Quantum Elec.* **2001**, *25*, 229.
(29) Prasad, P. N.; Williams, D. J. *Introduction to nonlinear optical effects in molecules and polymers;* Wiley: New York, 1991.
(30) *Molecular Electronics;* Jortner, J., Ratner, M., Eds.; Blackwell Science: Oxford, 1997.
(31) Kanis, D. R.; Ratner, M. A.; Marks, T. J. *Chem. Rev.* **1994**, *94*, 195−242.
(32) Brédas, J. L.; Adant, C.; Tackx, P.; Persoons, A.; Pierce, B. M. *Chem. Rev.* **1994**, *94*, 243−278.
(33) Karna, S. P. *J. Phys. Chem. A* **2000**, *104*, 4671−4673.
(34) Bernholc, J. *Phys. Today* **1999**, 30−35.
(35) Jonsson, D.; Ruud, K.; Taylor, P. R. *Comput. Phys. Commun.* **2000**, *128*, 412−433.
(36) van Gisbergen, S. J. A.; Schipper, P. R. T.; Gritsenko, O. V.; Baerends, E. J.; Snijders, J. G.; Champagne, B.; Kirtman, B. *Phys. Rev. Lett.* **1999**, *83*, 694−697.
(37) van Faassen, M.; de Boeij, P. L.; van Leeuwen, R.; Berger, J. A.; Snijders, J. G. *Phys. Rev. Lett.* **2002**, *88*, 186401.
(38) Denbigh, K. G. *Trans. Faraday Soc.* **1940**, *36*, 936−948.
(39) Vickery, B. C.; Denbigh, K. G. *Trans. Faraday Soc.* **1949**, *45*, 61−81.
(40) Stout, J. M.; Dykstra, C. E. *J. Am. Chem. Soc.* **1995**, *117*, 5127−5132.
(41) Stout, J. M.; Dykstra, C. E. *J. Phys. Chem. A* **1998**, *102*, 1576.
(42) Sylvester-Hvid, K. O.; Åstrand, P.; Ratner, M. A.; Mikkelsen, K. V. *J. Phys. Chem. A* **1999**, *103*, 1818.
(43) Zhou, T.; Dykstra, C. E. *J. Phys. Chem. A* **2000**, *104*, 2204−2210.
(44) Silberstein, L. *Philos. Mag.* **1917**, *33*, 92.
(45) Applequist, J.; Carl, J. R.; Fung, K. F. *J. Am. Chem. Soc.* **1972**, *94*, 2952.
(46) Applequist, J. *J. Chem. Phys.* **1985**, *83*, 809−826. Erratum in **1993**, *98*, 7664.
(47) Bode, K. A.; Applequist, J. *J. Phys. Chem.* **1996**, *100*, 17820.
(48) de Vries, A. H.; van Duijnen, P. T.; Zijlstra, R. W.; Swart, M. *J. Elecron Spectrosc. Relat. Phenom.* **1997**, *86*, 49.
(49) Burnham, C. J.; Li, J.; Xantheas, S. S.; Leslie, M. *J. Chem. Phys.* **1999**, *110*, 4566.
(50) Torrens, F.; Sánchez-Marín, J.; Nebot-Gil, I. *J. Mol. Graph.* **1996**, *14*, 245−259.
(51) Soos, Z. G.; Tsiper, E. V.; Pascal, R. A., Jr. *Chem. Phys. Lett.* **2001**, *342*, 652−658.
(52) Jensen, L.; Schmidt, O. H.; Mikkelsen, K. V.; Åstrand, P.-O. *J. Phys. Chem. B* **2000**, *104*, 10462.
(53) Kongsted, J.; Osted, A.; Jensen, L.; Åstrand, P.-O.; Mikkelsen, K. V. *J. Phys. Chem. B* **2001**, *105*, 10243.
(54) Jensen, L.; Åstrand, P.-O.; Osted, A.; Kongsted, J.; Mikkelsen, K. V. *J. Chem. Phys.* **2002**, *116*, 4001.
(55) Applequist, J. *J. Chem. Phys.* **1973**, *58*, 4251−4259.
(56) Applequist, J. *J. Phys. Chem. A* **1998**, *102*, 7723−7724.
(57) Applequist, J.; Quicksall, C. O. *J. Chem. Phys.* **1977**, *66*, 3455−3459.
(58) Bocian, D. F.; Schick, G. A.; Birge, R. R. *J. Chem. Phys.* **1981**, *74*, 3660−3667.
(59) Applequist, J.; Sundberg, K. R.; Olson, M. L.; Weiss, L. C. *J. Chem. Phys.* **1979**, *70*, 1240−1246. Erratum in **1979**, *71*, 2330.
(60) Shanker, B.; Applequist, J. *J. Chem. Phys.* **1996**, *104*, 6109−6116.
(61) Applequist, J.; Bode, K. A. *J. Phys. Chem. A* **2000**, *104*, 7129−7132.
(62) Applequist, J. *J. Phys. Chem. A* **2000**, *104*, 7133−7139. Erratum in **2000**, *104*, 10994.
(63) Levine, B. F.; Bethea, C. G. *J. Chem. Phys.* **1975**, *63*, 2666−2682.
(64) Sundberg, K. R. *J. Chem. Phys.* **1977**, *66*, 1475−1476. Erratum in *J. Chem. Phys.* **1977**, *67*, 4314.
(65) Buckingham, A. D.; Concannon, E. P.; Hands, I. D. *J. Phys. Chem.* **1994**, *98*, 10455.
(66) Jensen, L.; Sylvester-Hvid, K. O.; Mikkelsen, K. V.; Åstrand, P.-O. *J. Phys. Chem. A* **2003**, *107*, 2270.
(67) Birge, R. R. *J. Chem. Phys.* **1980**, *72*, 5312−5319.
(68) Thole, B. T. *Chem. Phys.* **1981**, *59*, 341.
(69) van Duijnen, P. T.; Swart, M. *J. Phys. Chem. A* **1998**, *102*, 2399.
(70) Jensen, L.; Åstrand, P.-O.; Sylvester-Hvid, K. O.; Mikkelsen, K. V. *J. Phys. Chem. A* **2000**, *104*, 1563.
(71) Buckingham, A. D. *Adv. Chem. Phys.* **1967**, *12*, 107.
(72) Buckingham, A. D.; Orr, B. J. *Quart. Rev.* **1967**, *21*, 195−212.
(73) Sundberg, K. R. *J. Chem. Phys.* **1977**, *66*, 114−118.
(74) Kwon,Y.-K.http://www.pa.msu.edu/ykkwon/Nanotubes/coordinates.html, 1998.
(75) Jensen, L.; Åstrand, P.-O.; Mikkelsen, K. V. *Nano Lett.* **2003**, *3*, 661.
(76) Bishop, D. M. *Rev. Mod. Phys.* **1990**, *62*, 343.
(77) Schulz, M.; Tretiak, S.; Chernyak, V.; Mukamel, S. *J. Am. Chem. Soc.* **2000**, *122*, 452.
(78) Jensen, L.; Åstrand, P.-O.; Mikkelsen, K. V. *J. Phys. Chem. B* **2004**, *108*, 8226.
(79) Jonsson, D.; Norman, P.; Ruud, K.; Ågren, H. *J. Chem. Phys.* **1998**, *109*, 572−577.
(80) Matsuzawa, N.; Dixon, D. A. *J. Phys. Chem.* **1992**, *96*, 6241−6247.
(81) Moore, C. E.; Cardelino, B. H.; Wang, X.-Q. *J. Phys. Chem.* **1996**, *100*, 4685−4688.
(82) Göller, A.; Grummt, U. W. *Int. J. Quantum Chem.* **2000**, *77*, 727.